International Journal of Fluid Power 7 (2006) No. 1 pp. 27-40

PUMP CONTROLLED ACTIVE ROLL STABILIZER

Anderson St. Hilaire, Jean-Claude Ossyra and Monika Ivantysynova

Purdue University, Department of Agricultural and Biological Engineering, 225 S. University Street, West Lafayette, IN 47907, USA
asthilai@purdue.edu, jossyra@purdue.edu, mivantys@purdue.edu

Abstract

The roll tendency of a vehicle can be significantly reduced if the stabilizer bar stiffness is actively controlled. Present electro-hydraulic solutions for vehicle active roll stabilization (ARS) use valve controlled actuators. An energy efficient pump controlled actuator concept for ARS is the focus of this research. This paper develops a non-linear model for the system and shows that the pump dynamics are sufficient for this actuator application. A simple control structure is developed from the linearized system model and the energy consumption of the system is determined for a realistic vehicle maneuver.

Keywords: displacement controlled actuator, swash plate control, Anti-roll bar, rotary actuator

1 Introduction

There is always a compromise in improving both the ride and roll comfort of a vehicle with a passive suspension system. The handling behavior of the majority of current vehicles is improved by using a passive stabilizer bar to reduce roll movement. The use of active stabilizer bars, first patented by Daimler-Benz in Germany in 1961 has proven to have many advantages over passive stabilizer bars. The active stabilizer bar is a two-piece shaft, one connected to the vane motor shaft and the other to its housing. The advantages include minimized body roll, better steering precision for the entire speed range and the ability to decouple the two shafts of the stabilizer bar. The body roll of the vehicle is minimized by actively applying an anti roll moment with the vane motor to the stabilizer bar during cornering. The vehicle can also achieve better steering precision by actively controlling the front and rear roll stiffness which affects the understeer characteristics of the vehicle. The ability to decouple the vane motor from the stabilizer bar allows for the system to eliminate the copying movement from one side of the vehicle to the next, which is experienced in a passive system during straight line driving on bumpy roads.

Figure 1 shows the full-automotive free body diagram used to model the dynamics of the system. The vehicle's mass is lumped at the center of mass and the tire and suspension are modeled as set of springs and dampers. The roll motion of the vehicle is the only degree of freedom permitted, and is generated by lateral forces acting on the center of mass. Other forces generated on the tire and suspension are modeled as disturbance moments on the system. The roll moment is assumed to act about the longitudinal direction (*x*-axis) while the anti-roll moment is generated by the twisting of the stabilizer bar about the lateral direction (*y*-axis).

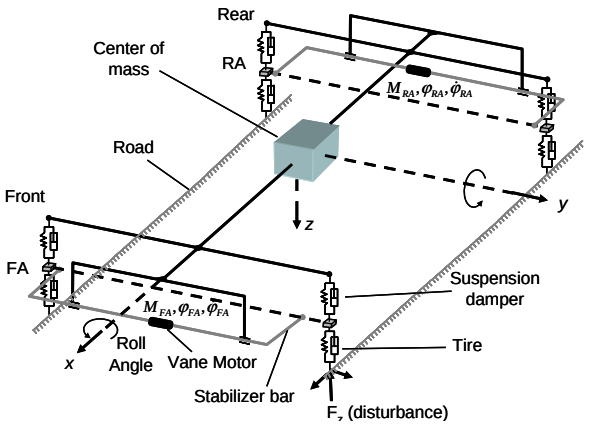

Fig. 1: *Scheme of vehicle using stabilizers in front and rear*

This manuscript was received on 10 October 2005 and was accepted after revision for publication on 26 January 2006

2 State of the Art

Over the past forty years active roll stabilizers have been developed and designed by automotive companies to improve vehicle handling. Many of these concepts, especially those developed in the 1960's and 1970's were not practical because of the lack of reliable sensing instruments and electrohydraulic components. In the mid 80's the intensity of research on ARS systems increased significantly, as can be noted by numerous patents submitted by automotive companies. Automotive companies such as BMW, Toyota, Peugeot and Nissan all obtained patents for proposed solutions in this period, (Wallentowitz and Konik, 1991). These proposals included roll stabilization systems with linear actuators as proposed by Nissan in 1985 and Mitisubishi in 1987 as well as systems with rotary actuators. The system presented by Lang and Walz (1991) showed through simulation and testing the feasibility of a rotary actuator in reducing vehicle body roll.

In 2000 BMW introduced the dynamic drive as an energy-optimized active roll stabilization system (Konik 2002). The design featured vane type rotary hydraulic actuators mounted on each of the stabilizer bars with torque controlled by two proportional pressure control valves (PPV). The differential pressure can be independently controlled for each motor with the help of two proportional pressure valves. The flow direction to the hydraulic motors (left or right axle) is ensured by a direction control valve (DCV) in Fig. 2. The system allows a driving condition dependent on distribution of the stabilization torques between front and rear axle. A special fail safe valve (FSV) is used to disconnect the front vane motor from the pressure source in failure cases, while two spring loaded check valves ensure low pressure in both chambers of the vane motor at all times. The system is currently implemented in the BMW 5 and 7 series.

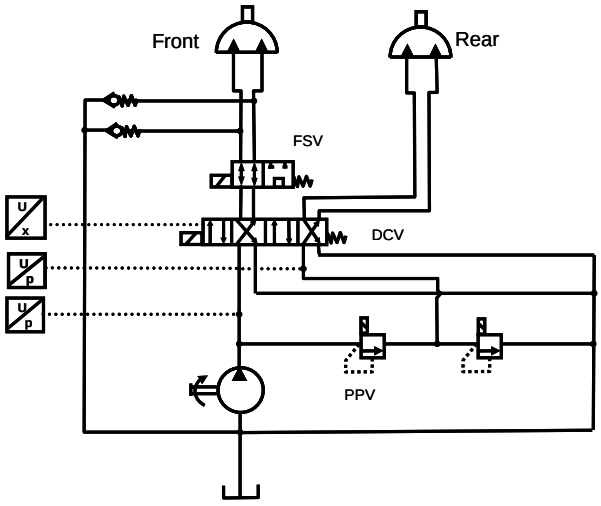

Fig. 2: *BMW dynamic drive hydraulic scheme*

To the authors' knowledge, all active roll stabilization systems which have been developed for vehicles use valves as the final controlling element. Valve controlled actuators are inherently inefficient due to throttling losses. In the system shown in Fig. 2 the main throttling losses occur in PPV. The energy loss is transformed into heat energy and has to be transferred out of the system by additional cooling effort. In addition, the implementation of a bulky valve block can be challenging for many automotive manufacturers.

An alternative to valve controlled actuators is displacement control using a variable displacement pump as final control element for controlling the motor torque, Grabbel (2004). Rahmfeld et al (2004) and Grabbel and Ivantysynova (2005) developed different applications for linear and rotary actuators based on this system concept.

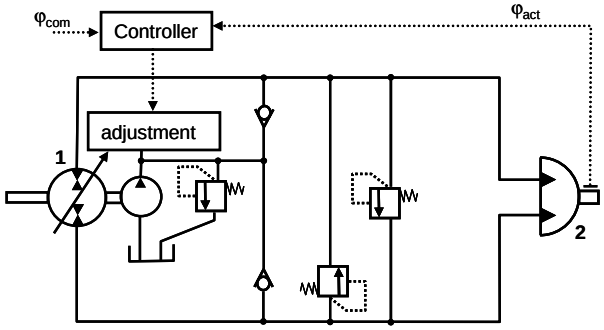

Fig. 3: *Displacement controlled rotary actuator (JIRA)*

Figure 3 displays the rotary pump controlled actuator concept successfully developed for robotic application by Grabbel and Ivantysynova (2001). The vane motor (2) is controlled by the variable displacement pump (1). The pump can be driven by either an electric motor or combustion engine.

The use of displacement control for active roll stabilization has many advantages. The major advantage of displacement control over valve control is the higher energy efficiency due to the absence of throttling losses within the main power lines of the actuator. Displacement control also allows for energy to be recovered from the system when the pump operates in the motoring mode. The recovered energy can be stored in an accumulator or used to drive other systems, such as the steering system. This paper will show that the achievable system bandwidth of the swash plate control is sufficient for the required actuator dynamics.

3 Solution for Pump Controlled Active Roll Stabilizer

The displacement controlled actuator concept shown in Fig. 3 allows for several system solutions when applied for active roll stabilization. Figure 4 shows one of the investigated solutions for the displacement controlled active roll stabilizer. For each axle (front/rear) a variable displacement pump (2) is used to control the torque of the vane motor (3), which is mechanically connected to the stabilizer bar. The servo pumps can be driven by the engine (1) or by an electric motor. In this paper two engine driven swash plate axial piston pumps are considered. The displacement of the pumps (2) is controlled using an electrohydraulic pump control system.

A charge pump (4) is used as a low pressure source. The charge pump (4) need not be added to the stabilizer system as an additional component.

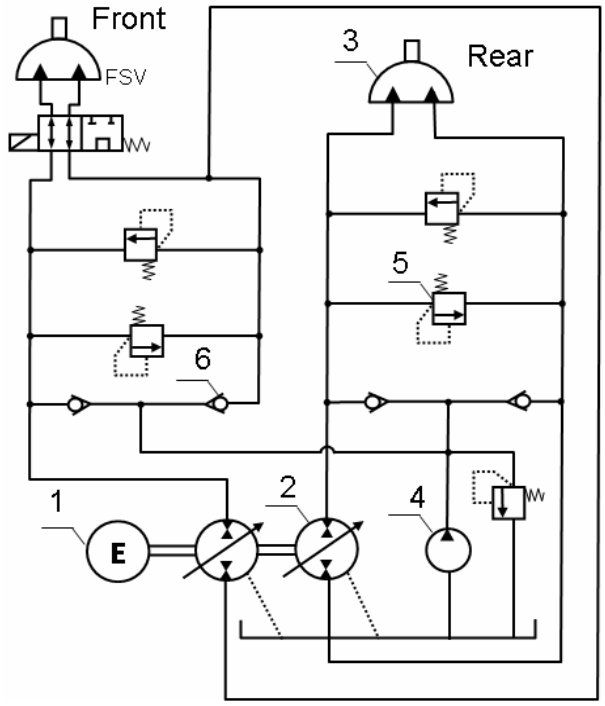

Fig. 4: *Pump controlled active roll stabilizer*

Assuming that there are other hydraulic systems installed in the car like a steering system, a common low pressure supply including the reservoir can be used for all of them. In case of a system failure a fail safe valve (FSV) is used to disconnect the vane motor of the front axle from the hydraulic circuit. Check valves (6) are used to ensure a low pressure level in the closed hydraulic circuit and pressure relief valves (7) are used to limit the maximum operating pressure in both lines.

For the pump controlled active roll stabilizer different types of variable displacement machines can be used, i.e. vane type pumps, radial piston and axial piston pumps. The use of a fixed displacement pump with a variable speed electric motor represents another solution. For the investigations presented a swash plate type axial piston pump has been used.

Considering the vehicle size and performance used for the valve controlled system (Fig. 2), the size of the vane type motor for the pump controlled system (Fig. 4) is the same. The pump is sized according to the required maximum angular velocity of the (fixed displacement) vane type motor for a minimum engine speed, which gives the maximum flow rate of the system. For the considered system a 1.8 cc pump has been chosen.

Figure 5 shows the basic structure of the electro-hydraulic pump control system with closed loop position control of the variable displacement pump, which serves as the final control element of the actuator. The pump control system requires very low flow, hence a single stage servo valve or single stage proportional valve is sufficient. Figure 5 shows the application of a so called direct drive valve using a linear electric motor as the electro-mechanical converter. The digital control of the pump is used also for implementation of the actuator control. The block diagram of the cascade structure is shown in section 5.

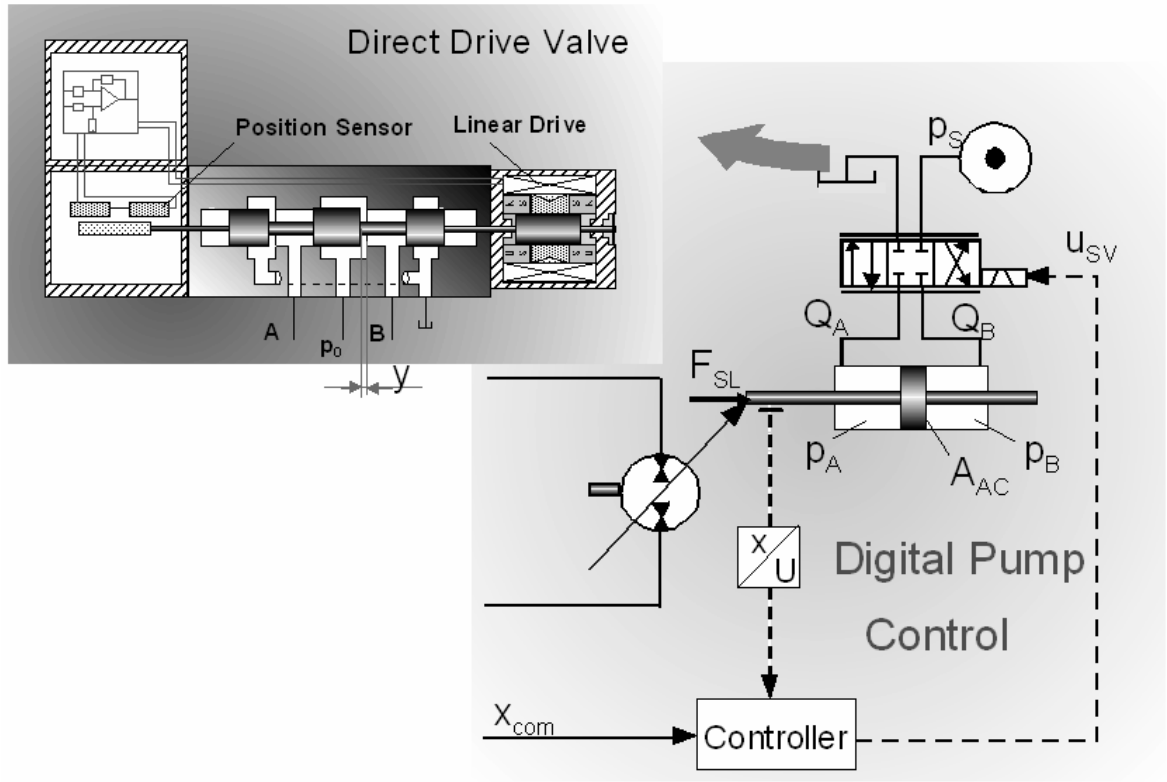

Fig. 5: *Simplified model of the servo pump control system*

4 Mathematical Model of the Active Roll Stabilizer

4.1 Pump Model

4.1.1 Pump Control System

Figure 6 shows a cross-section of a swash plate axial piston pump with an electro-hydraulic pump control system. The servo valve (1) controls the oil flow to and from the pump control cylinder (2), which is mechanically linked to the swash plate (3). A deflection of the swash plate out of its centred position in either direction increases the stroke of the pistons (5) and therefore the displacement volume of the pump. The direction of deflection defines the flow direction for given direction of shaft speed.

The centring spring (6) ensures the defined zero position of the swash plate when the pump is not running. The required flow rate for the pump control system is very small, i.e. a single stage servo valve or simple proportional valve can be used.

The basic dynamic model of the pump control system before performing further dominance analysis is based upon the equation of motion for the pump control cylinder, the pressure build-up equations for both chambers of the cylinder, including the volume of the connecting lines between the cylinder and the pump control valve, and the equation of motion for the control valve.

For the balance of forces, the inertia of all moveable parts (the swash plate, the pistons and the pump control cylinder) can be reduced to an equivalent mass, using the equivalency of rotational and translatory energy. All forces act directly on the control cylinder. The coordinates are defined achieving that a positive deflection of the servo valve spool y (to the left) results in a positive motion of the pump control cylinder x (to the right) and a positive pump flow.

The equation of motion of the pump control cylinder yields:

$$m_{\text{equ}} \cdot \ddot{x} = A_{\text{AC}} \cdot (p_{\text{A}} - p_{\text{B}}) - F_{\text{F}} - F_{\text{SL}} - F_{\text{SP}} \tag{1}$$

The friction force F_{F} of the cylinder is modelled as follows:

$$F_{\text{F}} = \underbrace{f_{\text{C}} \operatorname{sign}(\dot{x})}_{\textit{Coulomb}} + \underbrace{f_{\text{v}} \dot{x}}_{\textit{viscous}} + \underbrace{f_{\text{s}} e^{-\tau_{\text{s}}|\dot{x}|} \operatorname{sign}(\dot{x})}_{\textit{static}} \tag{2}$$

The force F_{SL} represents the main force which the pump cylinder must overcome to adjust a different displacement of the pump. More detailed calculation methods of this force can be studied in Ivantysyn and Ivantysynova (2003).

The pressure build-up inside each cylinder chamber of the pump control cylinder is determined by:

$$V_{\text{A}} \cdot \dot{p}_{\text{A}} = K_{\text{Oil}} \left(Q_{\text{A}} - A_{\text{AC}} \dot{x} - k_{\text{LA}} p_{\text{A}} - k_{\text{Li}} (p_{\text{A}} - p_{\text{B}}) \right), \tag{3}$$

$$V_{\text{B}} \cdot \dot{p}_{\text{B}} = K_{\text{Oil}} \left(Q_{\text{B}} - A_{\text{AC}} \dot{x} - k_{\text{LB}} p_{\text{B}} - k_{\text{Li}} (p_{\text{B}} - p_{\text{A}}) \right) \tag{4}$$

The cylinder chamber volumes are calculated from the current cylinder position x in relation to the middle position x_{H}. Additionally, the dead volume of the connections is considered:

$$V_{\text{A}} = V_{\text{dead}} + A_{\text{AC}} (x_{\text{H}} - x) \tag{5}$$

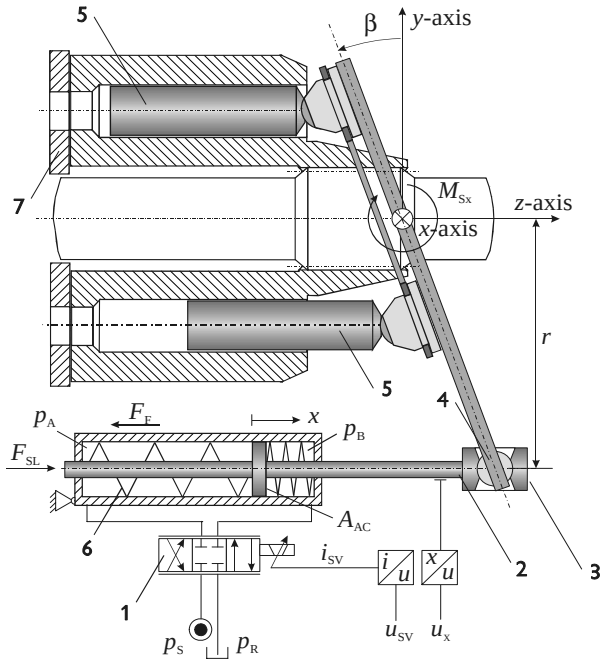

Fig. 6: *Servo pump with electro-hydraulic pump control system*

and

$$V_{\text{B}} = V_{\text{dead}} + A_{\text{AC}} (x_{\text{H}} + x) \tag{6}$$

The hydraulic capacitance is given by the ratio of chamber volume and bulk modulus. The hydraulic capacitance of both chambers is as follows:

$$C_{\text{H, A}} = \frac{V_{\text{A}}}{K_{\text{Oil}}} \text{ and } C_{\text{H, B}} = \frac{V_{\text{B}}}{K_{\text{Oil}}}. \tag{7}$$

The common hydraulic capacitance of both chambers yields

$$\begin{aligned} C_{\text{H}} &= \frac{1}{K_{\text{Oil}}} \left(\frac{1}{V_{\text{A}}} + \frac{1}{V_{\text{B}}} \right)^{-1} \\ &= \frac{1}{K_{\text{Oil}}} \left(\frac{A_{\text{AC}} x_{\text{H}} + V_{\text{dead}}}{2} + \frac{A_{AC}^2 x^2}{2(A_{\text{AC}} x_{\text{H}} + V_{\text{dead}})} \right) \end{aligned} \tag{8}$$

Assuming a servo valve with zero overlap the volume flow of the servo valve yields:

$$Q_{\text{A}} = \begin{cases} B \cdot y \sqrt{|\, p_{\text{S}} - p_{\text{A}} \,|} \operatorname{sign}(p_{\text{S}} - p_{\text{A}}) & \text{for } y \geq 0 \\ B \cdot y \sqrt{|\, p_{\text{A}} - p_{\text{R}} \,|} \operatorname{sign}(p_{\text{A}} - p_{\text{R}}) & \text{for } y < 0 \end{cases} \tag{9}$$

and

$$Q_{\text{B}} = \begin{cases} B \cdot y \sqrt{|\, p_{\text{B}} - p_{\text{R}} \,|} \operatorname{sign}(p_{\text{B}} - p_{\text{R}}) & \text{for } y \geq 0 \\ B \cdot y \sqrt{|\, p_{\text{S}} - p_{\text{B}} \,|} \operatorname{sign}(p_{\text{S}} - p_{\text{B}}) & \text{for } y < 0 \end{cases} \tag{10}$$

Where the servo valve constant B, which includes the discharge coefficient B = 3.8×10^{-3} $\text{m}^{0.5} \cdot \text{s} \cdot \text{kg}^{-0.5}$.

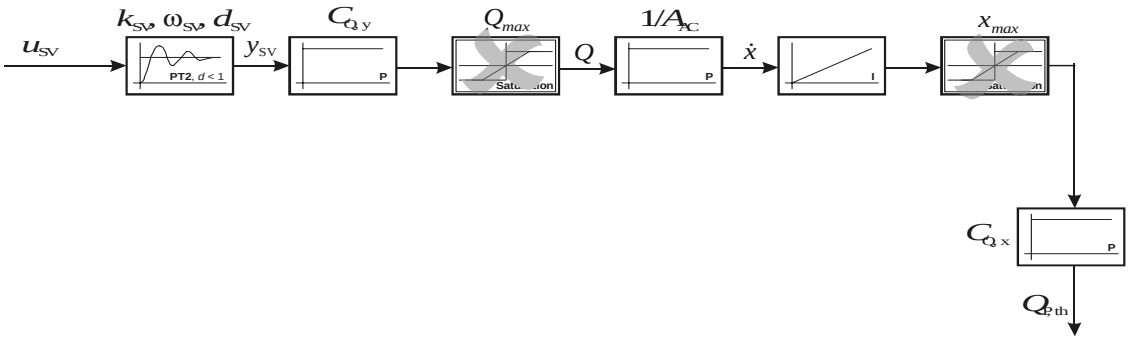

Fig. 7: *Simplified model of the servo pump control system*

Assuming there is no internal piston leakage on the pump control cylinder, we can write:

$$\begin{aligned} Q_{SV} &= Q_A = Q_B \\ &= B \cdot y \sqrt{\frac{|p_S - \Delta p|}{2}} \operatorname{sign}\left(p_S - \Delta p \operatorname{sign}(y)\right) \end{aligned} \tag{11}$$

using $\Delta p = p_A - p_B$ as the differential pressure of the pump control and assuming the reservoir pressure to be $p_R \approx 0$ bar. The equations for the pressure build-up can then be transformed to

$$\dot{p}_A = \frac{1}{C_{H,A}}\left(Q_A - A_{AC}\dot{x} - k_{LA}\,p_A - k_{Li}(p_A - p_B)\right) \tag{12}$$

and

$$\dot{p}_B = \frac{1}{C_{H,B}}\left(Q_B + A_{AC}\dot{x} - k_{LB}\,p_B + k_{Li}(p_A - p_B)\right) \tag{13}$$

For further simplification the pressure equations can be transformed to differential pressure, using

$$\Delta p = p_A - p_B \text{ and } Q_A = -Q_B, \tag{14}$$

where the external leakages have been neglected:

$$\Delta\dot{p} = \frac{1}{C_H}(Q_A - A_{AC}\dot{x} - k_{Li}\Delta p) \tag{15}$$

The state space equation based on Eq. (1) and Eq. (15):

$$\dot{x}_1 = \Delta\dot{p} = -\frac{A_{AC}}{C_H}\dot{x} + \frac{B}{C_H}\,y\sqrt{\frac{p_S - \Delta p}{2}} - \frac{k_{Li}\Delta p}{C_H}$$

$$\dot{x}_2 = x_3,$$

$$\dot{x}_3 = \frac{1}{m_{equ}}(A_{AC}\Delta p - F_F - F_{SL} - F_{SP}) \tag{16}$$

using the state vector $\boldsymbol{x} = \begin{bmatrix} \Delta p \\ x \\ \dot{x} \end{bmatrix}$ (17)

The valve dynamics can be sufficiently modelled by a second order system (PT_2 system). Assuming a second order system for description of the dynamic behaviour of the electro-mechanical converter of the valve and the spool we can write:

$$\ddot{y} + 2d_{SV}\omega_{SV}\dot{y} + \omega_{SV}{}^2 y = k_{SV}\omega_{SV}{}^2 u_{SV} \tag{18}$$

$$G(s) = \frac{k_{sv}}{\frac{1}{\omega_{sv}^2}\cdot s^2 + 2\cdot\frac{d_{sv}}{\omega_{sv}}\cdot s + 1} \tag{19}$$

where the valve gain is $k_{SV} = y_{SV,\,max}/u_{SV,\,max}$.

Different investigations (Berg 1999, Grabbel and Ivantysynova 2005) showed that the poles of the servo valve will nearly always dominate the pump control system open-loop characteristics, i.e the hydraulic eigenfrequency of the control cylinder with a range of 400 Hz up to 12,600 Hz is much higher than the eigenfrequency of servo valves used for pump control. The consequence of this relation is very important. The eigenfrequency and damping of the control valve dominate the pump control system characteristics.

The simplified model of the pump control system is shown in Fig. 7. The crossed blocks illustrate remaining system saturations which must be removed for a pure linear model. The transfer function for the complete pump control system is then reduced to a third order system, that represents the required parameters:

$$G_{AS,\,open}(s) = \frac{1}{s}\cdot\frac{C_y}{A_{AC}}\cdot\frac{k_{SV}}{\frac{1}{\omega_{SV}}\cdot s^2 + 2\cdot\frac{d_{SV}}{\omega_{SV}}\cdot s + 1} \tag{20}$$

Please note, this does not mean that the neglected parameters are irrelevant. It means that once the system is designed to achieve sufficient forces to overcome the swash plate moment and centring spring forces (when applicable), the *controller design* does not rely on these parameters.

Open loop characteristics of the servo pump control system are dominated by the dynamics of the servo valve used (ω_{SV}, d_{SV}, k_{SV}) and the gain of the pump control system, determined by the pump control cylinder area A_{AC}, the servo valve flow constant B and the supply pressure p_S, as derived before. It must be noted that especially the servo valve characteristics ω_{SV} and d_{SV} vary with respect to the commanded step size.

4.1.2 Loss Model

The prediction of the energy consumption of the proposed pump controlled actuator for active roll stabilization requires the consideration of a precise actuator loss model. In the case of pump control the main source of the losses occurs in the pump itself. Therefore, the

consideration of pump losses and their dependencies on operating parameters becomes very important. The reliability of the calculated effective volumetric flow rate of the pump depends on the accuracy of its steady state model in the whole parameter range.

The method proposed by Ivantysyn and Ivantysynova (1993) was used to determine the losses of this system. The method uses a pure mathematical approximation of measured curves and allows calculating very precise models independent of the type of displacement machine. The program POLYMOD, which was developed in the authors´ research group, has been used to determine coefficients and exponents of the polynomial for the approximation method (Mikeska 2002).

The mathematical description of the polynomial depends on the normalized values of the displacement volume $V_{\mathrm{i,norm}}$, the shaft speed n_{norm} and the pressure differential Δp_{norm}. The order of the values is represented by p as the order of polynomial displacement volume V_{i}, q as the order of polynomial shaft speed n and r as the order of polynomial pressure differential Δp. The polynomial with integer exponents for volumetric losses is described by:

$$Q_{\mathrm{S}} = Q_{\mathrm{S,norm}} \cdot \sum_{i=0}^{p}\sum_{j=0}^{q}\sum_{k=0}^{r} k_{\mathrm{Q,ijk}} \frac{V_{\mathrm{i}}^{i}}{V_{\mathrm{i,norm}}} \cdot \frac{n^{j}}{n_{\mathrm{norm}}} \cdot \frac{\Delta p^{k}}{p_{\mathrm{norm}}}, \qquad (21)$$

The mathematical description of the polynomial with integer exponents for hydro-mechanical losses is:

$$M_{\mathrm{S}} = M_{\mathrm{S,norm}} \cdot \sum_{i=0}^{p}\sum_{j=0}^{q}\sum_{k=0}^{r} k_{\mathrm{M,ijk}} \frac{V_{\mathrm{i}}^{i}}{V_{\mathrm{i,norm}}} \cdot \frac{n^{j}}{n_{\mathrm{norm}}} \cdot \frac{\Delta p^{k}}{p_{\mathrm{norm}}} \qquad (22)$$

The number of coefficients depends on the order of polynomial:

$$k_{num} = (p+1)\cdot(q+1)\cdot(r+1) \qquad (23)$$

Assuming the relation between the control cylinder position and the swash plate angle as linear and calculating the volumetric losses Q_{S} referring to Eq. 21, the flow rate of the servo pump is:

$$Q_{\mathrm{P,eff}} = \frac{x}{x_{\max}} \cdot V_{\mathrm{iP}} \cdot n_{\mathrm{P}} - Q_{\mathrm{S}} \qquad (24)$$

4.2 Vane Motor

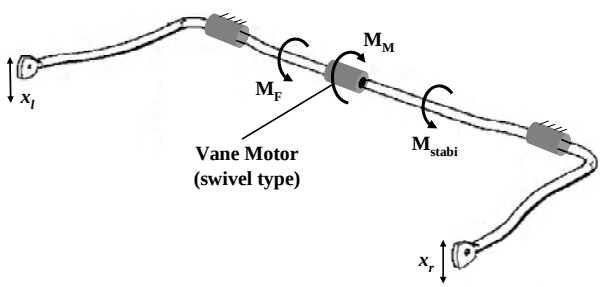

Fig. 8: *Simplified diagram of active stabilizer bar*

The equation of motion for the vane motor is based on a balance of momentum about the axis of the stabilizer bar, where all acting moments are summed (Fig. 8).

$$\Theta \cdot \ddot{\varphi} = M_{\mathrm{M}} - M_{\mathrm{Stabi}} - M_{\mathrm{F}}. \qquad (25)$$

The *stabilizer torque* M_{Stabi} depends on the spring stiffness c_{Stabi} of the stabilizer bar, the angular position of the vane motor φ, the spring travel of the wheel suspension system on the left side x_{l} of the axle and on its right side x_{r} and the lengths of the stabilizer bar l_{Stab}. It yields:

$$M_{\mathrm{Stabi}} = c_{\mathrm{Stabi}} \cdot \left[\varphi - \arcsin\left(\frac{x_{\mathrm{l}} - x_{\mathrm{r}}}{l_{\mathrm{Stab}}} \right) \right] \qquad (26)$$

The theoretical *shaft torque* M_{M} of the vane motor is derived from its displacement volume V_{M} and the pressure difference at low pressure and high pressure chamber:

$$M_{\mathrm{M}} = \Delta p \cdot \frac{V_{\mathrm{M}}}{2 \cdot \pi}. \qquad (27)$$

The *friction losses* M_{F} of a vane motor occur at the roller bearings of the motor shaft and at the sealing gaps, where the moving parts (vane and vane shaft) are sealed to the casing and the fixed case vane. A mathematical function for the friction torque model can be derived by the use of the Stribeck curve for modelling coulomb friction, viscous friction and static friction:

$$M_{\mathrm{F}} = r_{\mathrm{C}} \operatorname{sign}(\dot{\varphi}) + r_{\mathrm{V}}\dot{\varphi} + r_{\mathrm{H}} e^{-\tau_{\mathrm{H}}|\dot{\varphi}|} \operatorname{sign}(\dot{\varphi}) \qquad (28)$$

The problem, however, is the determination of the coefficients. The effective friction moment is dependent on a number of varying parameters, like dynamic load force and load direction (affecting the radial load on the roller bearings), dynamic load torque and vane position (affecting the pressure difference, the shaft pressure load and the flow conditions at the sealing gaps), oil viscosity (affecting the flow conditions at the sealing gaps) and others. Consequently, a precise loss model of the vane motor could only be taken from measurements of a high number of operating points, which is, on the other hand, not very reasonable for an efficient controller design process. For this reason the effect of variable friction parameters on the dynamic characteristics and therefore its consequence on the controller design process was studied. The torque losses of the vane motor has been changed between 2 and 5% of the theoretical torque. The effect on damping was still minor, see Table 3.

The pressure build-up of the main circuit can be modelled similar to the pressure build-up at a typical valve controlled hydraulic cylinder. However, two major differences have to be considered:

The effective volume flow is not significantly dependent on the load pressure, but only on the swash plate angle of the servo pump.

The pressure build-up only occurs in the high pressure line, while the low pressure level is pre-charged by an additional supply ($p_{\mathrm{LP}} \approx$ const., $\dot{p}_{\mathrm{LP}} \approx 0$).

The pressure build-up yields:

$$\begin{aligned}\Delta\dot{p}_{\mathrm{M}} &= (\dot{p}_{\mathrm{A,\ M}} - \dot{p}_{\mathrm{B,\ M}}) \\ &= \frac{1}{C_{\mathrm{H,\ M}}}\Sigma Q \\ &= \frac{1}{C_{\mathrm{H,\ M}}}\left(Q_{\mathrm{P},eff} - Q_{\mathrm{,MS}} - \frac{V_{\mathrm{M}}}{2\pi}\dot{\varphi}\right)\end{aligned} \tag{29}$$

4.2.1 Model of Hydraulic Lines

The distributed design of the proposed pump controlled actuators with engine driven pumps results in relatively long hydraulic lines, connecting the pump and motor. Especially the connection of the vane motor on the rear axle requires a long line. The oil volume of these lines has significant influence on the system dynamics. First, the hydraulic stiffness is reduced, since the hydraulic capacity increases with increasing oil volume. Second, the acceleration and deceleration forces acting on the oil mass increase, though it is expected that the acceleration and deceleration forces of the oil mass remain negligible, compared to the forces that correspond to the payloads of the stabilizer bar.

The compressible oil volume in the lines of the actuator cannot be neglected, where the hydraulic capacitance C_{H} influences the hydraulic poles´ eigenfrequency.

Basically, the oil volume is determined by the volume of the lines and the volume of the vane motor chambers. It has to be considered that the oil volume of both chambers of the vane motor is variable and depends on the current vane motor angle φ, since the oil volume inside the chambers of the vane motor changes with its shaft position. The fluid volume of the lines V_{L} remains constant and can be calculated as

$$V_{\mathrm{L}} = V_{\mathrm{LA}} = V_{\mathrm{LB}} = l_{\mathrm{L}} \cdot A_{\mathrm{L}} . \tag{30}$$

The variable chamber volume has to be calculated independently for both chambers, since it is dependent on the current vane motor shaft position:

$$V_{\mathrm{A,M}} = \frac{V_{\mathrm{M}}}{2\pi}\cdot(\varphi_n + \varphi) \text{ and } V_{\mathrm{B,M}} = \frac{V_{\mathrm{M}}}{2\pi}\cdot(\varphi_n - \varphi), \tag{31}$$

where φ_{n} marks the middle position. Finally the common hydraulic capacitance yields:

$$\begin{aligned}C_{\mathrm{H}} &= \frac{1}{K_{\mathrm{oil}}}\cdot\left(\frac{1}{V_{\mathrm{A,M}} + V_{\mathrm{L}}} + \frac{1}{V_{\mathrm{B,M}} + V_{\mathrm{L}}}\right)^{-1} \\ &= \frac{1}{K_{\mathrm{oil}}}\cdot\left(\frac{V_{\mathrm{L}} + \frac{V_{\mathrm{M}}}{2\pi}\cdot\varphi_n}{2} + \frac{\left(\frac{V_{\mathrm{M}}}{2\pi}\right)^2\cdot\varphi^2}{2\cdot\left(V_{\mathrm{L}} + \frac{V_{\mathrm{M}}}{2\pi}\cdot\varphi_n\right)}\right)^{-1}\end{aligned} \tag{32}$$

The *hydraulic inductance* describes the additional force that is required to accelerate or decelerate the oil mass enclosed in the hydraulic transmission line. This force is equivalent to an additional pressure difference $p_1 - p_2$ from the line entrance (p_1) to the end of the line (p_2):

$$(p_1 - p_2)\cdot A_{\mathrm{L}} = \rho \cdot l_{\mathrm{L}} \cdot A_{\mathrm{L}} \cdot \frac{dv}{dt} . \tag{33}$$

Substituting

$$A_{\mathrm{L}} \cdot \frac{dv}{dt} = \dot{Q}_{\mathrm{L}} \tag{34}$$

Eq. 34 can be expressed as:

$$\Delta p_{\mathrm{VL}} = p_1 - p_2 = \frac{\rho \cdot l_{\mathrm{L}}}{A_{\mathrm{L}}}\cdot\dot{Q}_{\mathrm{L}} \tag{35}$$

The pressure drop Δp_{VL} due to the flow of viscous fluid in the line depends on the flow velocity v_{L}, the kinematic viscosity of the fluid ν, the density of the fluid ρ and the flow resistance coefficient λ:

$$\Delta p_{\mathrm{VL}}(v_{\mathrm{L}},\ d_{\mathrm{L}},\ l_{\mathrm{L}}) = \frac{\rho}{2}\cdot v_{\mathrm{L}}^2 \cdot \frac{l_{\mathrm{L}}}{d_{\mathrm{L}}}\cdot\lambda \tag{36}$$

Regarding the Reynolds number

$$\mathrm{Re} = \frac{v_{\mathrm{L}} \cdot d_{\mathrm{L}}}{\nu} \tag{37}$$

and assuming a laminar flow within the lines

$$\lambda_{\mathrm{lam}} \approx \frac{64}{\mathrm{Re}}, \tag{38}$$

the pressure losses can be expressed as followed:

$$\Delta p_{\mathrm{VL}} = \frac{32\cdot\rho\cdot l_{\mathrm{L}}\cdot\nu\cdot v_{\mathrm{L}}}{d_{\mathrm{L}}^2} . \tag{39}$$

For simulation purposes, a pressure dependent loss model for the vane type motor is typically sufficient:

$$Q_{\mathrm{S,M}} \approx f(\Delta p) = k_{\mathrm{Li},\Delta\mathrm{p,M}}\cdot\Delta p . \tag{40}$$

The servo pump volumetric losses have the same importance to the plant damping characteristics as vane motor losses. When pressure supported vane motor seals are used, the pump losses may become dominant ($Q_{\mathrm{S,\ P}} > Q_{\mathrm{S,\ M}}$) and thus, the pump losses basically seals define the open-loop damping characteristics. This relation, however, depends on the actual volumetric efficiencies of pump and motor.

For linearization purposes it is necessary to reduce the volumetric loss model to pressure dependent losses only.

$$Q_{\mathrm{S,P}} = k_{\mathrm{Li},\Delta\mathrm{p,P}}\cdot\Delta p \tag{41}$$

For a common leakage model both leakages are added:

$$Q_{\mathrm{S}} = \left(k_{\mathrm{Li},\Delta\mathrm{p,M}} + k_{\mathrm{Li},\Delta\mathrm{p,P}}\right)\cdot\Delta p = k_{\mathrm{Li},\Delta\mathrm{p}}\cdot\Delta p \tag{42}$$

For the plant characteristics, especially the effective damping ratio of the open loop, the leakage (of motor and pump) is very important.

Figure 9 shows the block diagram of the main hydraulic circuit for the complete nonlinear model. The servo pump as the final control element is shown as a nonlinear block and represents the servo pump model, which can be used at different stages of simplification.

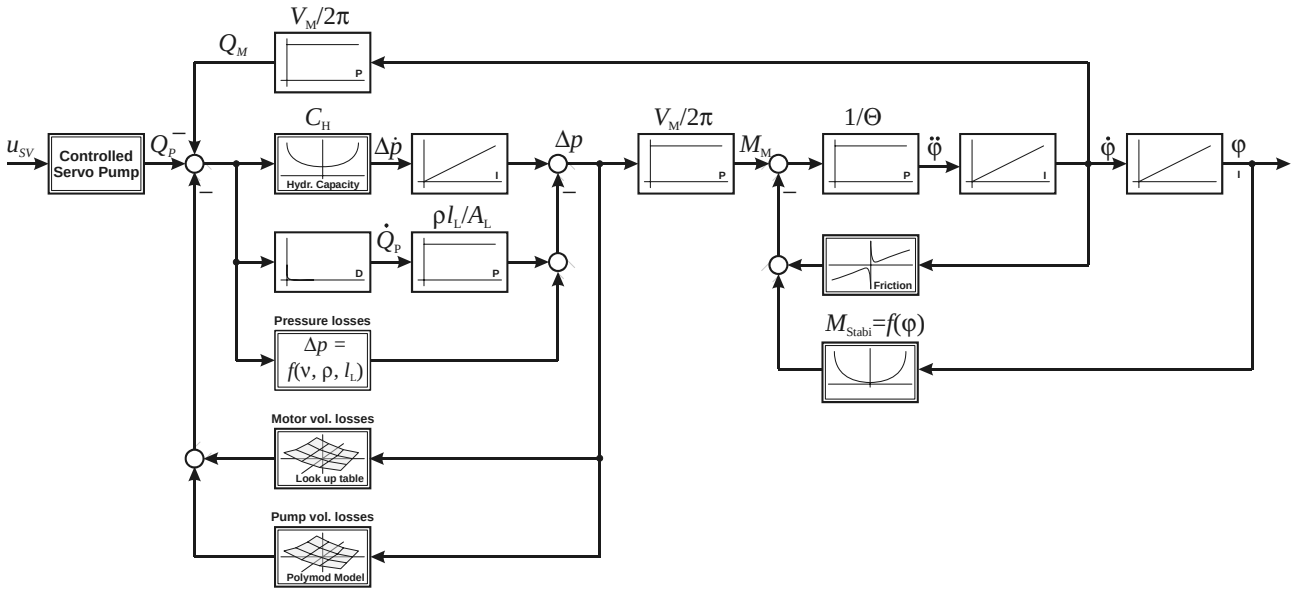

Fig. 9: *Non-linear plant*

4.2.2 Linearized State Space Model

For fixed-value controller design, based upon linear theory, a formally linear model is required for further analysis and controller synthesis. Equations 43 and 44 are the linearized state space model of the actuator.

The friction can be linearized by using only the viscous (velocity dependent) term. The load torque is modeled as a disturbance on the system. Further, the integration from velocity to position adds simply a third pole at the origin. For analysis it is sufficient to use the second order model (from the effective servo pump volumetric flow as input to the actuator velocity as output):

$$\mathbf{A}=\begin{bmatrix} -\dfrac{k_{Li,\Delta p}}{C_H} & -\dfrac{V_M}{2\cdot\pi\cdot C_H} \\ \dfrac{V_M}{2\cdot\pi\cdot\Theta} & -\dfrac{r_v}{\Theta} \end{bmatrix},\quad \mathbf{B}=\begin{bmatrix} \dfrac{V_{iP}\cdot n_P}{x_{max}\cdot C_H} \\ 0 \end{bmatrix}, \qquad (43)$$

$$\mathbf{C}=[0 \quad 1],\quad \mathbf{D}=\mathbf{0}.$$

using the state vector $\boldsymbol{x}=\begin{bmatrix} \Delta p \\ \dot{\varphi} \end{bmatrix}$. (44)

4.2.3 Size of Model

The sizes of the components are summarized in Table 1. As discussed in section 2 they were sized for use in a mid-size class vehicle, which requires a maximum torque for roll stabilization $M_{roll,max}$ = 1400 Nm at the stabilizer bar and therefore at the vane type motor, which gives the displacement of the motor under consideration of the maximum differential pressure in the system of Δp_{max} = 180 bar. Based on the requirement of the maximum angular position, which has to be reached in a certain time, the maximum effective flow rate can be calculated. Considering an engine speed of 3000 rpm the maximum required displacement volume of the pump is 1.8 cc.

Table 1: Component sizes for front axle

Max. motor displacement	5.24×10^{-4}	V_M [m^3]
Max. pump displacement	1.8×10^{-06}	V_p [m^3]
Servo valve freq. (±10%, - 3dB)	420 (65)	ω_{sv} [rad/s](Hz)
Servo pump freq. (±25%)	280 (45)	[rad/s](Hz)
Front stabilizer stiffness	5700	Nm/rad
Stabilizer bar length	0.15	[m]
Max. stabilizer bar angle	±14.46	φ_{max} [°]
Max. stabilizer bar angular velocity	57.5	$\dot{\varphi}$ [°/s]
Line volume	2.62×10^{-4}	V_L [m^3]

For the pump model, scaling laws were used in order to determine the loss behaviour and for sizing the pump control system. Though the chosen valve dynamics can also be realized with valves used for larger pump sizes, it displays the possibility to use inexpensive single stage valves. The authors are aware of the possibility to incorporate high dynamics valves with a small flow rate, similar to those used in engine combustion control. However they are not state of the art presently and do not have a high influence on the present results. For the simulation results only the front axle system has been considered.

5 Control Strategies

Driving comfort is subjective and this gives the engineer some flexibility in determining the system performance. In general the ARS system should have a sufficiently fast response time in all modes of operation, minimum overshoot and no oscillatory behaviour during settling. In all the previously mentioned requirements, the speed of response is the most important demand. Darling J. et al (1992) showed that a 12 Hz system bandwidth is necessary to reduce vehicle roll by a factor of 4 for severe steer step inputs. The perform-

ance requirements dictate that position control of the actuator is sufficient. Control of the system velocity is not required since accurate trajectory control is not essential.

The overall control strategy is to use a two cascade control concept (Fig. 10). The inner loop consist of the swash plate control, which is considered as integrated into the servo pump, and the outer loop is the angular position control of the stabilizer bar (vane motor). The system position control signal can be derived from a laterally sensitive acceleration sensor placed slightly ahead of the vehicle centre of gravity. This allows the acceleration sensor to measure a combination of the lateral and yaw acceleration, Darling and Hickson (1998). Alternatively, measurements of vehicle speed and steer velocity can also be used to derive a position control signal. The feedback signal can be measured with an angular sensor placed on the stabilizer bar to determine the twist angle. Another possibility is to measure the stabilizer bar's end displacement with a linear transducer, where kinematics can be used to relate actuator linear position to actuator twist angle.

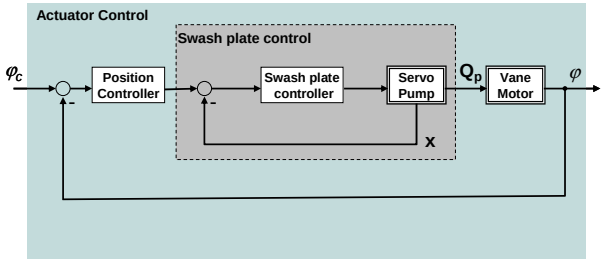

Fig. 10: *Block diagram for control system with cascade structure*

To develop a robust controller to attain the specified performance, an upper and lower bound of the varying parameters which affect the plant dynamics must be determined. Table 2 shows the range of the varying parameters considered in this simulation. Simulations determined that the engine speed and the torque losses in the vane motor are the varying parameters with the greatest influence on the plant dynamics. Table 3 shows the influence of all these parameters on the hydraulic poles frequency and damping ratio. Increasing the engine speed increases the response time of the uncontrolled plant. The torque loss in the vane motor has an influence on the damping of the hydraulic poles.

Table 2: Uncertain parameters of ARS system

Parameter	sym	Unit	Min	Max
Coef. of Leakage	K_{Li}, ΔP	$m^3/s/Pa$	4×10^{-13}	2×10^{-12}
Hydraulic Cap.	C_H	m^3/Pa	4×10^{-14}	8×10^{-14}
Moment of inertia	Θ	kgm^2	0.1	.25
Coef. friction moment.	r_v	Nms	6.5	26.5
Engine speed	n	rpm	1500	6000

Table 3: Range of hydraulic frequency and damping ratio of hydraulic poles

Parameter	sym	Unit	Min	Max
Frequency	ω_H	rad/s	686	1320
Damping ratio	d_H	-	.037	.139

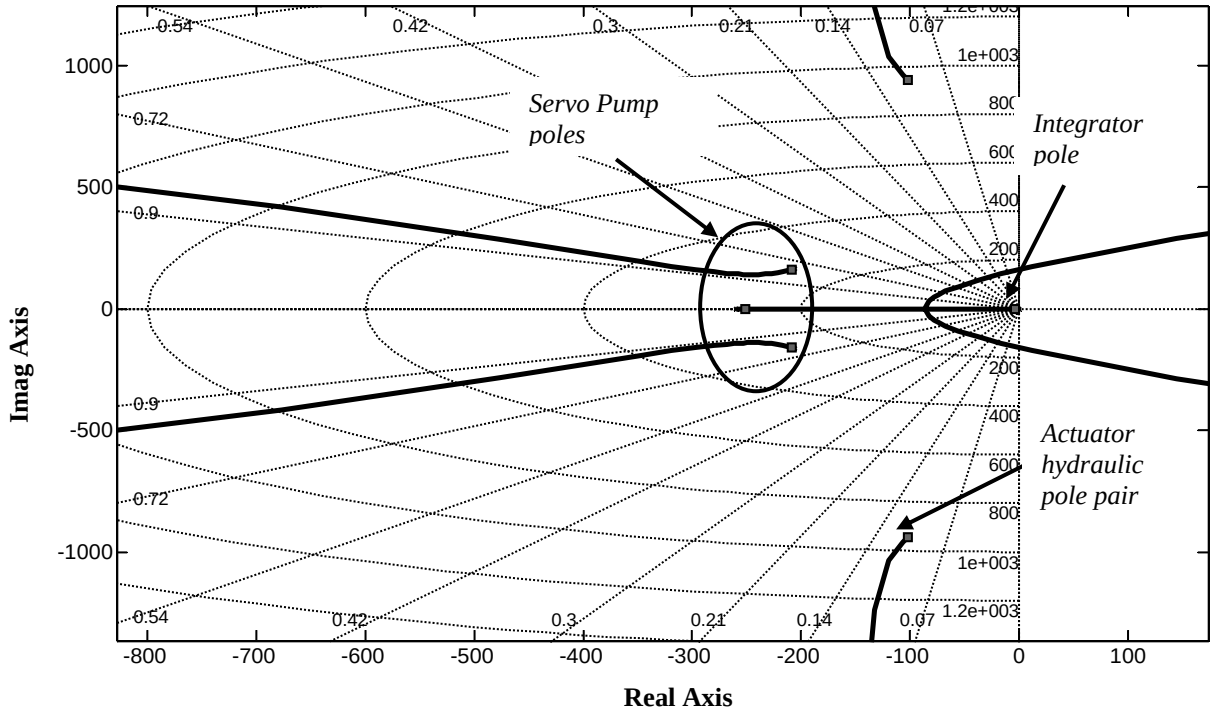

Fig. 11: *Root locus of nominal system (freq. is in rad/s)*

Figure 11 shows the root locus plot of the linearized system. The hydraulic pole pair has a high frequency and very low damping. The low damping of the hydraulic poles is a common occurrence in pump controlled hydraulic system. Notice the servo pump poles have a lower frequency than the hydraulic poles. The nature of the plant allows for the system to be controlled by simple proportional gain. Increasing the system gain increases the speed of response of the system to the specified performance value. The influence of the hydraulic poles on the system speed of response is not significant because of their high frequency. However, these high frequency poles could potentially create noise or flow pulsations in the system.

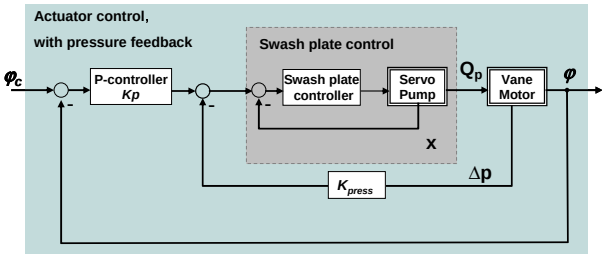

Fig. 12: *Block diagram for control system with dynamic pressure feedback*

Dynamic pressure feedback (Fig. 12) and 2nd order compensators (see Fig. 13) are two common compensation strategies that are used to increase the damping of the hydraulic poles. Implementation of these compensating strategies to improve the damping of the system proved futile for this particular system. To realize a 2nd order compensator, the microprocessor speed has to be sufficient to cancel the effects of the hydraulic poles. This may not be the most economical solution to the car manufacturer.

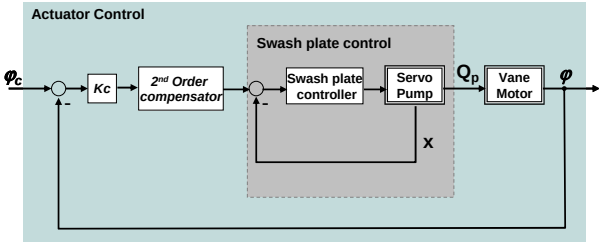

Fig. 13: *Block diagram for control system with 2nd order compensator*

The typical advantage of dynamic pressure feedback is that only the system pressure has to be measured and since pressure sensors are already implemented to monitor the system pressure this poses no additional sensor effort. Grabbel (2003) showed how pressure feedback improved the damping of a particular displacement controlled rotary actuator by moving the hydraulic poles to a region of higher damping, though it has to be mentioned, that the hydraulic poles were at a lower frequency compared to the present displacement control system. This strategy was successful because the servo pump frequency was significantly higher than that of the underdamped hydraulic poles. For the ARS system presently investigated, the use of pressure feedback is not possible as the servo pump poles are not fast enough to compensate for the demands on the pump. It is clear from this investigation that pressure feedback can increase damping only for displacement controlled systems in which the frequency of the servo pump is much greater than that of the dominant hydraulic poles.

Figure 14 shows the Bode diagram of the proportionally controlled system. It can be observed that for small angles the linear and non-linear responses are nearly equivalent. We see for large angle displacements the system deviates from the linear model. The Ackermann parameter space method was used to determine a robust controller gain for all the system varying parameters. The parameter space method is a well-developed design approach for determining fixed controller gains which satisfy the system performance for all operating points. The true strength of this method lies in its ability to determine simultaneously stable gains for more complex controller structures. Although proportional control always produces a steady-state error to disturbances, nonlinear simulation of the system showed a steady-state error less than 0.5 percent.

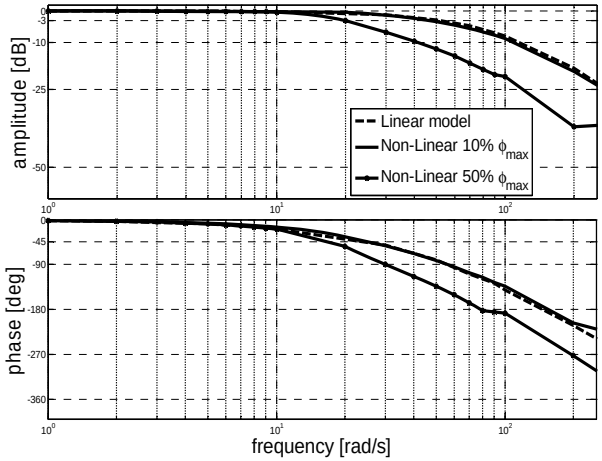

Fig. 14: *System response in Bode diagram*

6 Simulation Results

Before discussing simulations results for proving the function of the control concept and the energy consumption of this new actuator, it should be pointed out that the authors tested a similar actuator for robotic applications in a previous project. For that project, a large test rig was built to perform a series of measurements on a vane type pump controlled actuator. For this reason the authors chose not to build a new test rig for performing measurements for the proposed stabilizer actuator system at this stage of the project. Further details for previously performed measurements can be found in Grabbel (2003).

The simulations have been performed under Matlab/Simulink by the use of the non-linear model described in section 3. Only the roll stabilizer system of the front axle has been considered. In Fig. 15 a typical drive situation for a vehicle has been used to define a drive cycle. The vehicle drives with a vehicle velocity around 120 km/h in a S-curve with unsteady curve

radius for the first half of the manoeuvre and a steady curve radius for the second half of the manoeuvre. Due to the kinematics of the vehicle body, the roll stabilizer requires a certain angular position (middle position is zero) to compensate the forces acting on the stabilizer bar in order to reduce the roll motion of the vehicle. The commanded angular position for the roll stabilizer controller is displayed over the simulation time in Fig. 15 under the assumption that a central vehicle dynamic controller calculates this value according to the present driving situation. Please note, the illustration on the right side of Fig. 15 is simplified and does not show the exact simulated S-Curve described above.

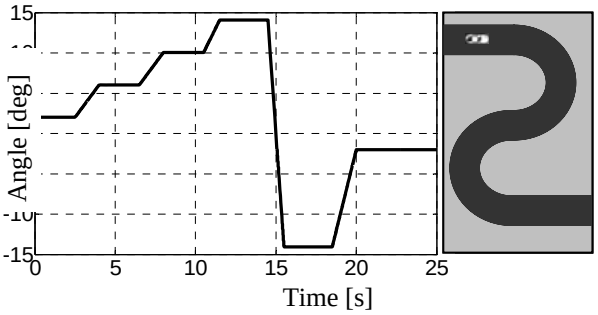

Fig. 15: *Simulated drive cycle*

Due to the unsteady curve radius, the commanded angular position for the motor of the roll stabilizer system has to be readjusted several times for the first 14 seconds of the simulation. It then changes to the opposite direction within 2 seconds, showing the change of curve direction, and returns to a steady position due to a steady curve radius.

Figure 16 displays the simulation results for the required output power of the front axle stabilizer system for this manoeuvre on the vane type motor shaft over the simulation time.

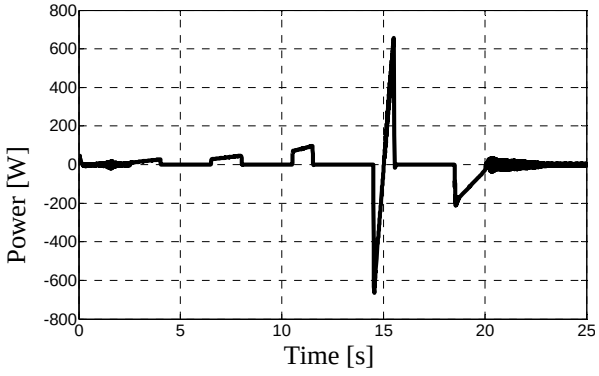

Fig. 16: *Motor output power over simulation time.*

It is clear that the output power of the motor is only required if the commanded angular position (Fig. 15) changes. The maximum power level depends on the absolute value of the change of the command angular position. Due to the change of curve direction (second 14 to second 18) output power is assigned as negative, which equals a recovery of energy, while the stabilizer bar loads the motor and helps it to achieve its new position. Here the vane type motor operates in pumping mode, allowing energy recovery by running the pump in motoring mode and driving the shaft of the engine.

In Fig. 17 the output power of the pump at the combustion engine is displayed over simulation time. This is the power required for the front axle roll stabilizer system for the simulated manoeuvre.

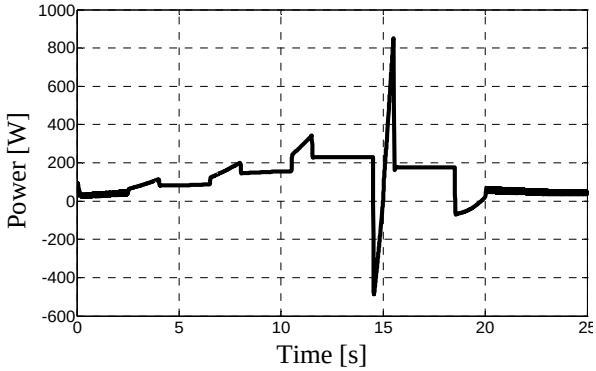

Fig. 17: *Pump output power on engine side over simulation-time.*

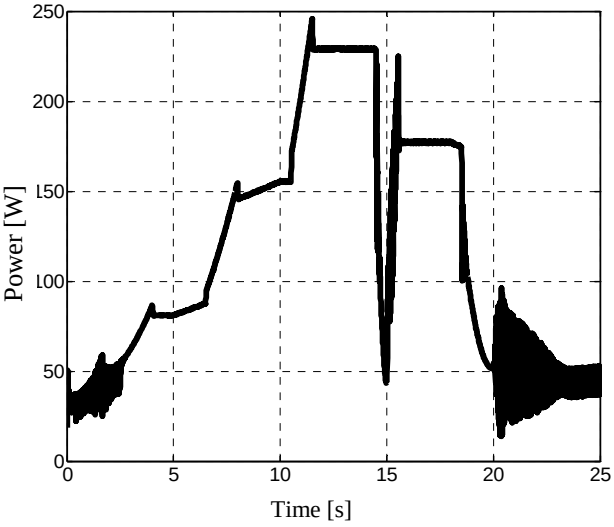

Fig. 18: *Pump power loss over simulation time.*

The power consumption of the pump indicates that power is required if the commanded angular position (Fig. 15) changes and also for maintaining a steady position of the motor. This effect shows the influence of the loss behaviour of the pump, which is displayed in Fig. 18 over simulation time. The required output power level is higher than the required output power of the motor. Nevertheless, the change of curve direction (second 14 to second 18) allows pump operation in motoring mode in order to recover energy at the combustion engine, which can be used for the actuation of other vehicle accessories, e.g. fan drive, pumps etc. while the combustion engine injection can be reduced or possibly stopped.

The loss behaviour in Fig. 18 shows a strong dependency on the flow rate (high angular position for motor, Fig. 14) of the roll stabilizer system for the simulated manoeuvre.

7 Conclusions

The developed alternative solution for an active roll stabilization system in automobile application shows a high potential for system simplification compared to valve actuated systems. It also contributes to fuel savings because the main losses are at the pump and motor and it has the ability to recovery energy in certain cases.

The assumed pump dynamics are sufficient for this actuator application. The required system responses, which are known from valve actuated system solutions, are mainly dependent on the valve dynamics of the pump control system. The pump control is considerably smaller than the valve used for the valve actuated system solutions. Therefore, higher dynamics can be achieved.

For the controller design different control strategies have been presented and compared. Due to the fact that the fequency of the hydraulic system poles of the stabilizer system is considerably higher than the poles for the pump control system (the final control element) it is not possible to enhance the behaviour of a fixed gain angular position control concept in a cascade structure, which showed a steady-state error less than 0.5 percent in non-linear simulation. Measures to damp the hydraulic system poles by the use of pressure feedback or 2nd order compensator are not useful due to the dynamic limitation of the pump control system valve for this special application with the assumed valve dynamics.

Simulation results for a typical driving situation (S-curve at 120 km/h) showed that the required power for the combustion engine to operate the active roll stabilization system is minimized, only covering the load dependent pressure losses of the hydraulic machines and also recovering energy in cases when the motor operates as a pump, which can be used to drive vehicle accessories.

The realization of the proposed energy saving actuator for active roll stabilization as proposed in this paper is generally possible. Vane type motors which are mounted at the stabilizer bar in the front or rear axle already exist in valve actuated systems. The pumps for actuating the front axle and rear axle roll stabilizer can be mounted directly on the engine, which helps also to encapsulate the noise. The use of belt drives for driving the pumps can be exploited to change their size if it is required. Long lines will be used to connect the pump and the motor of the rear axle. The third pump (charge pump) of the active roll stabilizer system can be shared by other vehicle accessories like a hydraulic suspension system or the steering system. This centralized approach also simplifies the maintenance of the active roll stabilization system.

Nomenclature

β	swash plate angle	[°]
Δ_{pvl}	pressure drop due to flow of viscous fluid	[Pa]
Θ	effective inertia of the stabilizer bar	[kgm²]
ω_{SV}	eigenfrequency of the servo valve	[rad/s]
φ	angular position of stabilizer bar	[°]
φ_c	commanded stabilizer angle	[°]
A_{AC}	piston area	[m²]
c_{stabi}	spring coefficient	[N/m]
B	servo valve constant	$[(m^5/kg)^{1/2}]$
C_H	hydraulic capacitance	[m/N]
$C_{H,A}$	hydraulic capacitance of chamber A	[m/N]
$C_{H,B}$	hydraulic capacitance of chamber B	[m/N]
$C_{H,M}$	hydraulic capacitance of main circuit	[m/N]
C_y	flow gain	[m²/s]
d_{SV}	servo valve damping	[-]
f_C	coefficient of Coulomb friction	[N]
f_s	coefficient of static friction	[N]
f_v	coefficient of viscous friction	[Ns/m]
F_F	friction force	[N]
F_{SP}	spring force	[N]
F_{SL}	force resulting from swash plate moment.	[N]
k_{LA}	coefficient of external leakage of chamber A	[m³/s/Pa]
k_{LB}	coefficient of external leakage of chamber B	[m³/s/Pa]
k_{Li}	coefficient of internal leakage	[m³/s/Pa]
k_{SV}	servo valve amplification	[m/V]
K_{Oil}	oil bulk modulus	[N/m²]
m_{equ}	effective mass of the swash plate system with respect to the adjustment cylinder	[kg]
M_F	friction losses in Vane motor	[Nm]
M_{stabi}	stabilizer bar Torque	[Nm]
p_A	cylinder pressure in chamber A	[Pa]
p_B	cylinder pressure in chamber B	[Pa]
p_R	return line pressure	[Pa]
p_S	pump control system supply pressure	[Pa]
Q_A	volume flow to chamber A	[m³/s]
Q_B	volume flow to chamber B	[m³/s]
Q_{sv}	leakage flow	[m³/s]
r	cylinder lever arm	[m]
r_c	coefficient of Coulomb friction moment	[Nm]
r_H	coefficient of static friction moment	[Nm]
r_v	coefficient of viscous friction moment	[Nm/°]
u_{SV}	servo valve control voltage	[V]
u_x	output signal of pump control cylinder position sensor	[V]
u_{SV}	servo valve input voltage	[V]
V_A	volume of cylinder chamber A	[m³]
V_B	volume of cylinder chamber B	[m³]
V_{dead}	dead volume of cylinder, including lines	[m³]
x	piston position of pump adjustment cylinder	[m]

x_H	neutral (centred) position of the adjustment cylinder	[m]
x_l	Spring travel wheel suspension system (left side)	[m]
x_r	Spring travel wheel suspension system (right side)	[m]
y	spool position of the pump control valve	[m]
y_{sv}	spool position at operating (= linearization) point	[m]

A	system matrix
B	input matrix
C	output matrix
D	feedthrough matrix with index $_{AS}$ for adjustment system
x	state vector of state space model
x_1 .. x_3	individual elements of the state vector

G(s)	transfer function

References

Ackermann, J. et al. 2000. Robust Control – Systems with Uncertain Physical Parameters. Springer, London, UK.

Berg, H. and **Ivantysynova, M.** 1999. Design and testing of a robust linear controller for secondary controlled hydraulic drive. Journal of Systems and Control Enginering. Proceedings of the Institution of Mechanical Engineers Vol. 213 Part I, pp. 375-386.

Berg, H. 1999. Robuste Regelung verstellbarer Hydromotoren am Konstantdrucknetz, Dissertation, Gerhard-Mercator-Universität Duisburg, Germany. Fortschritt-Berichte VDI, Reihe 8, No. 764, VDI Verlag, Düsseldorf, Germany.

Darling, J., Dorey, R. E, Ross-Martin, T. J. 1992. A low cost active anti-roll suspension for passenger cars. Journal of Dynamics Systems, Measurement, and Control Vol. 114, pp.599-605.

Darling, J., Hickson, L.R. 1998. An Experimental Study of a Prototype Active Anti-Roll Suspension System. Vehicle Systems Dynamics, Vol. 29, pp. 309-329.

Grabbel, J. and **Ivantysynova M.** 2001. Control strategies for Joint Integrated Servo Actuators in mobile machinery. 7th Scandinavian International Conference on Fluid Power, Linköping, Sweden.

Grabbel, J. and **Ivantysynova, M.** 2005. Advanced swash plate control for high dynamics of displacement controlled actuators. International Journal of Fluid Power, Vol. 6 (2005) No. 2, pp. 19-36.

Grabbel, J. 2003. Robust Control Strategies for Displacement Controlled Rotary Actuators using Vane Type Motors. Dissertation, Technical University of Hamburg-Harburg, Germany. Fortschritt-Berichte VDI, Reihe 8, No. 1029, VDI Verlag, Düsseldorf, Germany.

Ivantysyn, J. and **Ivantysysnova, M.** 1993. Hydrostatische Pumpen und Motoren. (German) 1. Aufl., Würzburg: Vogel Verlag.

Ivantysyn, J. and **Ivantysynova M.** 2000. Hydrostatic Pumps and Motors - Principles, Designs, Performance, Modelling, Analysis, Control and Testing. Academica Books International, New Delhi.

Ivantysynova, M. et al. 2002. Prediction of Swash Plate Moment Using the Simulation Tool CASPAR. International Mechanical Engineering 2000 Congress and Exposition, IMECE2002-39322, New Orleans, Louisiana, USA.

Konik, Dieter. 1991. Development of the Dynamic Drive for the new 7 series of the BMW Group. Int. Journal of Vehicle Design, Vol. 28, Nos. 1/2/3, pp. 131-149.

Lang, R. and **Walz, U.** 1991**.** Active Roll Reduction, EAEC 3rd Int. Conf. on Vehicle Dynamics and Powertrain Engineering, 11-13 June, Strasbourg.

Mikeska, D. 2002. A precise steady-state model of displacement machines for the application in virtual prototyping of power-split drives. 2nd FPNI-PhD Symposium Modena 2002, University of Modena, Italy.

Rahmfeld, R. 2002. Development and Control of Energy Saving Hydraulic Servo Drives for Mobile Systems. Dissertation, Technical University of Hamburg-Harburg, Germany. Fortschritt-Berichte VDI, Reihe 12 No. 527, VDI Verlag, Düsseldorf, Germany.

Rahmfeld, R. et al. 2004. Displacement Controlled Wheel Loader – a simple and clever Solution. Proc. of the 4th International Fluid Power Conference (4. IFK), Dresden, Germany, Vol. 2, pp. 183-196.

Wallentowitz, H. and **Konik, D.** 1991. Actively Influenced Suspension Systems – Survey of Actual Patent Literature, EAEC 3rd Int. Conf. on Vehicle Dynamics and Powertrain Engineering, 11-13 June, Strasbourg.

Wieczorek, U. and **Ivantysynova, M.** 2002. Computer Aided Optimization of Bearing and Sealing Gaps in Hydrostatic Machines - the Simulation Tool CASPAR. International Journal of Fluid Power 3 (2002) No. 1, pp. 7-20.

Anderson St. Hilaire

Born on April 20th 1979 in the Commonwealth of Dominica, West Indies. He received his B.S. degree from New Mexico State University in Las Cruces, New Mexico with high honors in Mechanical Engineering in 2003. Since August 2004 he is a Masters student at Purdue University West Lafayette, Indiana, in the area of Automatic controls and Mechatronics.

Jean-Claude Ossyra
Born on October 30th 1971 in Gelsenkirchen (Germany). He received his Eng. Diploma Degree in Mechanical Engineering from the Gerhard Mercator University of Duisburg, Germany, and his PhD. Degree in Fluid Power from the Technical University of Hamburg-Harburg, Germany. Since September 2004 he is a visiting scholar at Purdue University, USA. His main research areas are energy saving control concepts for vehicle drive line and modeling, simulation and testing of fluid power systems.

Monika Ivantysynova
Born on December 11th 1955 in Polenz (Germany). She received her MSc. Degree in Mechanical Engineering and her PhD. Degree in Fluid Power from the Slovak Technical University of Bratislava, Czechoslovakia. After 7 years in fluid power industry she returned to university. In April 1996 she received a Professorship in fluid power & control at the University of Duisburg (Germany). From 1999 until August 2004 she was Professor of Mechatronic Systems at the Technical University of Hamburg-Harburg. Since August 2004 she is Professor in Mechnical Engineering and Agricultural and Biological Engineering at Purdue University, USA. She was approved as Maha named Professor in Fluid Power Systems and director of the Maha Fluid Power Research Center at Purdue University in November 2004. Her main research areas are energy saving actuator technology and model based optimization of displacement machines as well as modeling, simulation and testing of fluid power systems. Besides the book "Hydrostatic Pumps and Motors" published in German and English, she has published more than 90 papers in technical journals and at international conferences.